Ground and Excited States of Zinc Phthalocyanine Studied by Density Functional Methods

G. Ricciardi and A. Rosa*

Dipartimento di Chimica, Università della Basilicata, Via N. Sauro 85, 85100 Potenza, Italy

E. J. Baerends*

Afdeling Theoretische Chemie, Vrije Universiteit, De Boelelaan 1083, 1081 HV Amsterdam, The Netherlands

Received: November 17, 2000; In Final Form: February 27, 2001

The first *time-dependent DFT* study of the excited states of ZnPc is presented. The theoretical results provide an accurate description of the UV−vis and vacuum−UV spectra and prove to be in excellent agreement with gas-phase spectra and generally in line with deconvolution analyses of solution and Ar/matrix absorption and MCD spectra. The nature and intensity of the main spectral features are highlighted and interpreted on the basis of the ground state electronic structure of the complex. A fragment approach where the four benzopyrrole rings and the aza bridges are taken as building blocks has proven to be a very important tool to fully understand the energy and composition of the MOs involved in the transitions and, from these, the excitation energies and intensities. The Gouterman a_{1u} orbital is the HOMO and the assignment of the Q band is conventional and uncontroversial. The B band comprises five E_u excitations, whose positions and intensities are in very good accordance with the deconvolution of the experimental absorption band performed with the help of MCD spectra. However, this deconvolution invokes Jahn−Teller splitting of the E_u states which we have not calculated. We find at the red edge of the B band the weak 2nd $\pi\rightarrow\pi^*$ transition and at the blue edge the weak $n\rightarrow\pi^*$ transition which have been identified in the experiments. We do not confirm at low energy, in the tail of the Q band (the "Q_{02}" region) an electronic origin for the band which has been suggested to arise from the lowest *z*-polarized $n\rightarrow\pi^*$ transition. This transition is predicted by our calculations to be very weak and to lie in the B band region. The energies and intensities of the higher excitations are in excellent agreement with the UV N and L bands and with the far UV C and X bands. The predicted level pattern of the lowest triplet excited states fits in with phosphorescence data available and excited-state absorption spectra.

Introduction

Metallophthalocyanines (MPcs) have been studied extensively since the beginning of the century. These highly stable macrocyclic π-systems display interesting properties such as light stability and efficient light absorption in the red and visible region of the spectrum that make them potential candidates for applications in optoelectronics, photoconducting materials,[1−3] and photosensitizers for photodynamic therapy (PDT).[4,5] In view of the possible applications, a considerable effort has been devoted to the characterization of the excited states of metallophthalocyanines, their derivatives, and assemblies thereof by a variety of optical spectrometric techniques including circular dichroism (CD) magnetic circular dichroism (MCD), fluorescence spectroscopy, and, in recent years, time-resolved optical spectroscopies. Among metallophthalocyanines, ZnPc has received special attention. The initial motivation was that ZnPc is ideally suited for the characterization of the excited states of the Pc ring. Due to the d^{10} configuration of the central Zn^{2+} ion the optical spectra of ZnPc complexes are not complicated indeed by the "additional" MLCT and LMCT bands appearing in the spectra of other transition metal phthalocyanines, yet the D_{4h} symmetry of MPcs is retained. More recently, the discovery that Zn gives phthalocyanines valuable fluorescence and singlet oxygen production properties, which allow their use in the detection and treatment of tumors, has renewed the interest in the spectroscopic properties of ZnPc and its peripherally substituted derivatives.[4,5]

To date a number of experimental studies of the excited states of ZnPc are available, including gas phase,[6] thin film,[7] solution,[8,9] and argon matrix[10] absorption spectra, solution,[8,9] and argon matrix[10] MCD spectra, solution luminescence spectra,[11] luminescence, and magnetic circularly polarized luminescence (MCPL) spectra in an argon matrix.[11]

The gas-phase spectrum of ZnPc was reported some 30 years ago by Edwards and Gouterman[12] who identified five bands, Q, B, N, L, and C, in the 800−200 nm (1.5−6.2 eV) UV−vis region and two bands, X_1 and X_2, at 180 nm (6.89 eV) and 160 nm (7.75 eV) respectively in the vacuum UV region. SCMO−PPP−CI calculations[12] showed that the first four E_u excited states accounting for the Q, B, N, and L bands are, unlike in porphyrins, relatively pure single electron $\pi-\pi^*$ transitions, whereas multitransition excited states describe the higher energy region of the spectrum.

The first detailed band envelope deconvolution analyses of the room temperature solution absorption and MCD spectra of ZnPc(L) complexes, where L is an axially coordinated cyanide, imidazole or pyridine ligand, was reported by Nyokong et al. in 1987.[8] The analyses of the spectra led to the identification of five bands, Q, B_1, B_2, N, and L, corresponding to doubly degenerate states. More recently, Mack and Stillman[9] through band deconvolution of absorption and MCD spectra of (CN)ZnPc(−2) recorded at cryogenic temperatures were able to provide a detailed deconvolution of the complete B band into five underlying transitions. In addition to the Q, B, and N bands

10.1021/jp0042361 CCC: $20.00
Published on Web 05/04/2001

they identify a low intensity band at 2.05 eV (604 nm), just to the blue of the Q-band, which is ascribed, in agreement with VanCott et al.,[10] to an $n\rightarrow\pi^*$ transition linking the e_u aza-nitrogen lone pair orbital with the e_g LUMO.

Absorption and MCD data for ZnPc isolated in a Ar/matrix over a very wide energy range, 700−135 nm (1.77−9.1 eV), were reported by VanCott et al.[10] The use of matrix isolation and its accompanying low temperature afforded well-defined spectra over the entire region, providing a clear characterization of the energy and symmetry of many more excited states than identified in the absorption and MCD solution spectra of ZnPc complexes.[8,9] The clear correlation existing between the ZnPc/Ar and the gas-phase spectra of Edwards and Gouterman induced VanCott et al. to still retain the Q, B, N, L, C, X_1, and X_2 gas-phase band notation, with the understanding that these labels indicate spectral regions rather than single bands.

Although spectral band deconvolution analysis of the absorption and MCD spectra gives indications on the energy, number, and magnetic moment of the excited states contributing to each spectral region, accurate quantum mechanical calculations are required to fully characterize the excited states.

A compelling need for accurate calculations of the excited states of ZnPc in a very wide energy range, including the still theoretically unexplored vacuum UV region, has been expressed already long time ago by VanCott et al.[10] who could only correlate their Ar/matrix ZnPc spectra to very old SCMO−PPP−CI calculations of the excited states of CuPc.[13] Since then many theoretical investigations have appeared concerning the excited states of MPcs, including ZnPc. Most of these studies are based on semiempirical models which require the use of adjustable parameters (see ref 14 for a review of these calculations). The few available transition state[15,16] and ΔSCF[17] density functional theory (DFT) calculations on the excited states of MPcs do not account properly for the considerable configuration mixing occurring in these systems. The only first principles accurate calculations which have appeared to date on the excited states of phthalocyanines are the SAC-CI (symmetry adapted cluster configuration interaction) calculations of the lowest excited states of free base phthalocyanine by Toyota et al.[18] and our time-dependent density functional (TDDFT) calculations of the excited states of NiPc.[19]

With the aim to afford an accurate description of the electronic spectrum of ZnPc, we study here the excited states of this complex using time-dependent density functional theory which provides a first principles method for the calculations of excitation energies and many related response properties within a density functional context.

For applications to large molecules, TDDFT methods are an excellent alternative to conventional highly correlated ab initio methods such as SAC-CI, STEOM-CC (similarity transformed equation-of-motion coupled cluster), and CASPT2 (complete active space SCF plus second-order perturbation theory) for which calculations of the excited states of transition metal phthalocyanines are still a challenge. The reliability of TDDFT approach in obtaining accurate predictions of excitation energies and oscillator strengths is by now well documented for a wide range of molecules, ranging from small molecules[20−24] to large organic molecules,[25,26] higher fullerenes,[27] as well as, more recently, metal carbonyls,[28,29] free base porphin,[30] and transition metal tetrapyrroles.[19,31] The obtained results are competitive in accuracy with available highly correlated ab initio results.

Before dealing with the excited states of ZnPc, we elucidate the ground state electronic structure of this molecule using a fragment approach where the four indol rings and the aza bridges are taken as building blocks of the phthalocyanine ring. This approach is a powerful tool to predict the changes in energy and intensity of the spectral features upon variation of the macrocycle framework, as proven in the case of the Ni(II) tetrapyrrole series we have recently investigated,[19] or upon the perturbation induced by electron donor or electron acceptor peripheral substituents. Our analysis of the ground-state electronic structure is based on Kohn−Sham molecular orbitals of DFT. As extensively discussed in a recent paper,[19] the Kohn−Sham orbital model is very suitable for interpretation of the electronic structure and elucidation of the character of the excitations. The use of Kohn−Sham orbitals affords a direct connection with the many LCAO-MO treatments based on semiempirical or Hartree−Fock orbitals, while having at the same time the advantage of the high accuracy of the TDDFT treatment of the excitation energies.

Method and Computational Details

The computational method we use is based on the time-dependent extension of density functional theory. TDDFT is thoroughly reviewed in refs 20 and 32−34.

In our implementation,[35,36] the solution of the TDDFT response equations proceeds in an iterative fashion starting from the usual ground-state or zeroth-order Kohn−Sham (KS) equations.[35] For these one needs an approximation to the usual static exchange-correlation (xc) potential v_{xc} (**r**). After the ordinary KS equations have been solved, the first-order density change has to be calculated from an iterative solution to the first-order KS equations. In these first-order equations an approximation is needed to the first functional derivative of the time-dependent xc potential v_{xc} (**r**, *t*) with respect to the time-dependent density $\rho(\mathbf{r}', t')$, the so-called xc kernel.[34,37,38] For the xc kernel, we use the Adiabatic Local Density Approximation (ALDA). In this approximation, the time dependence (or frequency dependence if one talks about the Fourier transformed kernel) is neglected, and one simply uses the differentiated static LDA expression. In our case we use the Vosko-Wilk-Nusair parametrization.[39]

For the exchange-correlation potentials which appear in the zeroth-order KS equations we use the recent model KS exchange-correlation potential v_{xc}^{SAOP} which is constructed with a statistical average of different model potentials for occupied KS orbitals (SAOP).[40,41] Specifically, the potential may be written as a sum of model potentials v_i^{mod} which are each strongly weighted in a region where an orbital density $\rho_i(\mathbf{r}) = n_i|\varphi_i(\mathbf{r})|^2$ dominates:

$$v_{xc}^{SAOP}(\mathbf{r}) = \sum_i^{occ} \frac{\rho_l(\mathbf{r})}{\rho(\mathbf{r})} v_i^{mod}(\mathbf{r})$$

The model potentials v_i^{mod} have the form

$$v_i^{mod}(\mathbf{r}) = a_i v_{xc}^{LB\alpha}(\mathbf{r}) + (1 - a_i) v_{xc}^{GLLB}(\mathbf{r}); \qquad a_i = \exp[-2(\epsilon_{HOMO} - \epsilon_i)^2]$$

The v_i^{mod} asymptotically have the required $-1/r$ behavior (which the LDA and GGA potentials lack) since they acquire asymptotically the form of the LBA potential,[42] which has this behavior. In the inner region, notably in the atomic inner shells, the GLLB potential[43] dominates which approximates the shape of the exact Kohn−Sham potential with proper steplike behavior when going from one shell to the next inner shell. This step behavior is lacking in the LDA and GGA potentials. The SAOP

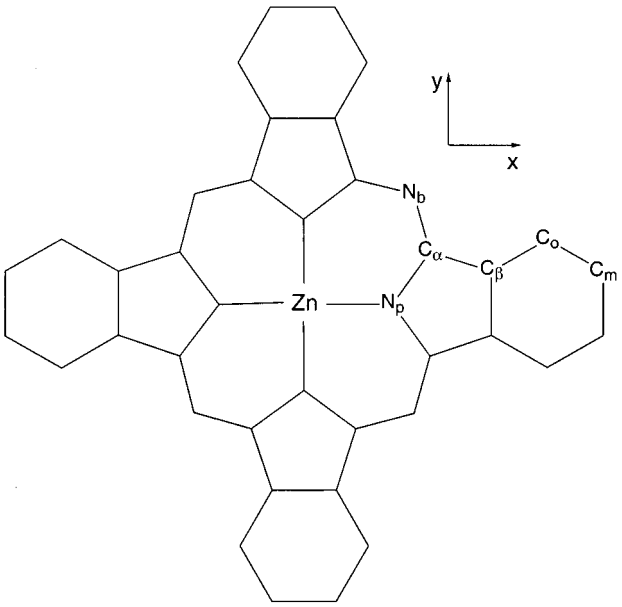

Figure 1. Atom labeling scheme for ZnPc.

TABLE 1: Optimized and Experimental Bond Distances (Å) and Angles (deg) for ZnPc

	calcd	exp[a]
$Zn-N_p$	2.006	1.980(2)
N_p-C_α	1.377	1.369(2)
$C_\alpha-C_\beta$	1.463	1.455(2)
$C_\beta-C_\beta$	1.415	1.400(3)
$C_\alpha-N_b$	1.335	1.331(2)
$C_\beta-C_o$	1.397	1.393(3)
C_o-C_m	1.399	1.391(3)
C_m-C_m	1.410	1.396(3)
$C_\alpha-N_b-C_\alpha$	124.5	123.5(2)
$C_\alpha-N_p-C_\alpha$	109.9	109.1(2)
$C_\beta-C_\alpha-N_p$	108.4	108.8(2)
$C_\beta-C_\beta-C_\alpha$	106.7	106.6(2)
$C_\beta-C_o-C_m$	117.9	117.3(2)
$C_o-C_m-C_m$	121.1	121.5(2)

[a] Data from ref 48. The numbers in parentheses are the estimated standard deviations.

potential thus by construction provides a balanced description of the electron exchange and correlation in both outer and inner atomic and molecular regions. High quality results for a wide variety of response properties of prototype molecules have been obtained using v_{xc}^{SAOP}.[41] More recently, this potential has been successfully used in ground- and excited states calculations of transition metal tetrapyrroles.[19]

The calculations have been performed for the symmetry and spin allowed A_{2u} and E_u states up to 8.0 eV and for the lowest symmetry allowed triplet states.

All calculations reported in this paper have been performed with the ADF−RESPONSE module[36] which is an extension of the Amsterdam Density Functional (ADF) program system.[44−46] It has many features in common with the underlying ADF code and has similar scaling and parallelization characteristics.

For the calculations we made use of the standard ADF IV basis set[47] which is an uncontracted triple-ζ STO basis set, with one 3d polarization function for the C and N and one 2p for H atoms, and a triple-ζ nd, $(n + 1)$s basis with one $(n + 1)$p function for Zn. The cores (C, N: 1s; Zn: 1s−2p) were kept frozen.

The calculations have been performed for the D_{4h} optimized geometry of the molecule. For the analysis of molecular orbitals

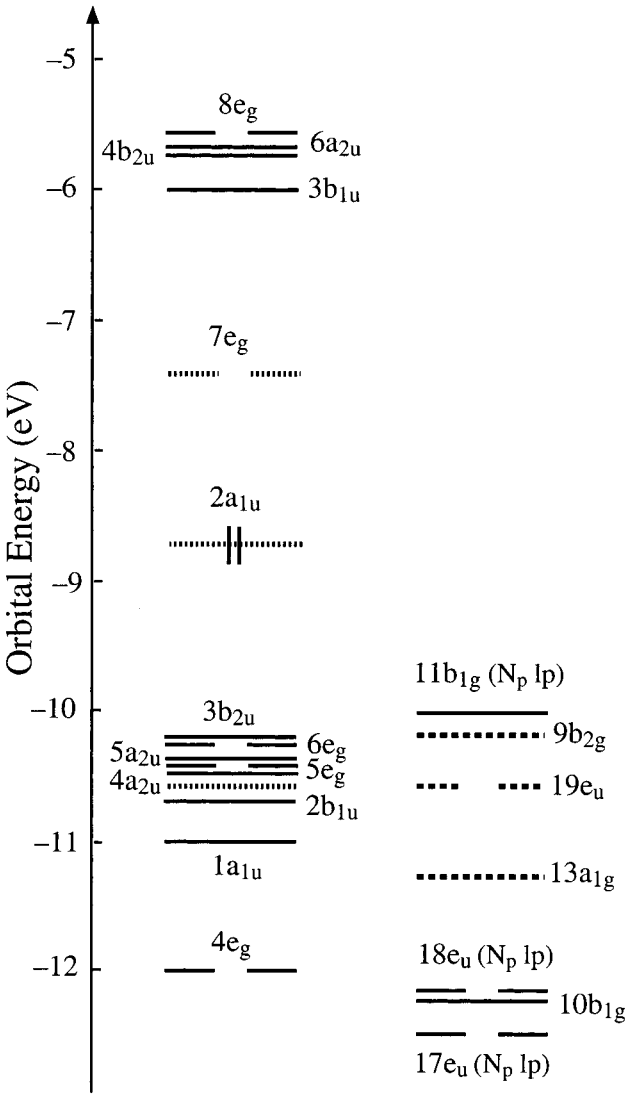

Figure 2. Energy level scheme of ZnPc. Double occupancy is indicated for the HOMO only. All lower lying levels are also doubly occupied. The Gouterman's four orbitals are indicated with hatched lines and the N_b lone pair orbitals of a_{1g}, b_{2g}, and e_u symmetry are indicated with dashed lines.

in terms of constituting fragment orbitals, the fragments have been taken in exactly the geometry they have in the total molecule. The orientation of the molecule and the atom labeling is shown in Figure 1. For the chemically distinctive classes of bond lengths and bond angles the optimized values are reported in Table 1 together with the experimental[48] ones averaged in agreement with D_{4h} geometry.

Ground State Electronic Structure Analysis

In Figure 2, the ground state one-electron levels of ZnPc are shown. For sake of clarity, the Gouterman four orbitals, hereafter simply denoted as "G" orbitals, are indicated with hatched lines. The highest N lone pair levels are given in the second column. The set of bridging aza (N_b) lone pair, of a_{1g}, b_{2g}, and e_u symmetry, are indicated with dashed lines. An atomic orbital population analysis of these and of the Zn based orbitals, the very low lying 3d and the high lying 4,5 s and 4p, is also given in Table 2. We will first discuss the relevant π levels, and next the aza bridge and pyrrolic nitrogen lone pairs.

The π Orbitals. In a recent study[19] concerning the ground and excited states of NiP (P = porphyrin), NiPz (Pz =

TABLE 2: Percentage Contribution of Individual Atoms to MOs of ZnPc

MOs	E (eV)	Zn	N_p	C_α	C_β	N_b	C_o	C_m	H
				unoccupied orbitals					
$7a_{2u}$	−3.26	64.0 ($4p_z$)	2.0	14.0	7.0	5.0	5.0	2.0	1.0
$15a_{1g}$	−3.33	47.0 (4,5s)							53.0
$14a_{1g}$	−3.69	68.0 (4,5s)							32.0
:	:	:	:	:	:	:	:	:	:
$8e_g$	−5.56		6.0	5.0	12.0	3.0	54.0	17.0	3.0
$6a_{2u}$	−5.67	5.0 ($4p_z$)	3.0	6.0	6.0	5.0	56.0	16.0	3.0
$4b_{2u}$	−5.77		14.0	16.0	4.0		46.0	15.0	5.0
$3b_{1u}$	−6.00			14.0	35.0	22.0	3.0	25.0	1.0
$7e_g$	−7.40		11.0	40.0	14.0	16.0	7.0	12.0	
				occupied orbitals					
$2a_{1u}$	−8.78		2.0	59.0	5.0		19.0	14.0	1.0
$11b_{1g}$	−10.04	12.0 ($d_{x^2-y^2}$)	66.0(l.p.)	11.0	11.0				
$9b_{2g}$	−10.18		12.0	10.0	4.0	74.0(l.p.)			
$3b_{2u}$	−10.18		21.0		38.0			36.0	5.0
$6e_g$	−10.22		24.0	2.0	35.0	2.0	3.0	34.0	−
$5a_{2u}$	−10.35		1.0	1.0	42.0	14.0		40.0	2.0
$5e_g$	−10.42			1.0	17.0	8.0	53.0	19.0	2.0
$2b_{1u}$	−10.43			1.0	15.0	4.0	61.0	17.0	2.0
$4a_{2u}$	−10.51	4.0 ($4p_z$)	48.0	4.0	2.0	39.0		3.0	
$19e_u$	−10.59		11.0	9.0	9.0	71.0(l.p.)			
$1a_{1u}$	−10.91			17.0	25.0		46.0	10.0	2.0
$13a_{1g}$	−11.22		6.0	10.0	9.0	75.0(l.p.)			
$4e_g$	−11.96		20.0	31.0	7.0	22.0	8.0	12.0	
$18e_u$	−12.14	7.0 ($4p_\sigma$)	26.0(l.p.)	16.0	19.0	9.0	6.0	7.0	10.0
$10b_{1g}$	−12.21		4.0	6.0	30.0		14.0	17.0	29.0
$17e_u$	−12.46	7.0 ($4p_\sigma$)	26.0(l.p.)	3.0	18.0	3.0	9.0	12.0	22.0
:	:	:	:	:	:	:	:	:	:
$7b_{1g}$	−16.74	18.0 ($d_{x^2-y^2}$)		8.0	13.0	3.0	16.0	19.0	23.0
$5b_{2g}$	−16.83	84.0 (d_{xy})	2.0	6.0		2.0	2.0	2.0	2.0
$8a_{1g}$	−17.22	58.0 (d_z^2)		6.0	9.0	2.0	10.0	7.0	8.0
$1e_g$	−17.24	98.0 (d_π)	2.0						
$6b_{1g}$	−17.65	59.0 ($d_{x^2-y^2}$)	10.0(l.p.)	4.0	9.0		4.0	6.0	8.0
$7a_{1g}$	−17.72	31.0 (d_z^2)	8.0	2.0	15.0		21.0	9.0	14.0

porphyrazine), NiTBP (TBP = tetrabenzoporphyrin), and NiPc (Pc = phthalocyanine) tetrapyrrole series, we have shown that most of the features of the orbital level spectrum and the underlying electronic structure of the ring systems can be understood from a fragment approach where the four pyrrole (Py) or benzopyrrole (BzPy) rings and the methine or aza bridges are taken as building blocks. The same approach will be used here to elucidate the electronic structure of ZnPc.

Accordingly, we build up the phthalocyaninato ring using BzPy rings and aza bridges as fragments. The levels and the contour plots of the lowest π orbitals of the BzPy ring system are shown in Figure 3. These orbitals have been extensively discussed in ref 19 in terms of a pyrrolic π electron system perturbed by the fused benzene and here we will only briefly recall their relevant features.

The lowest BzPy orbital of Figure 3, the nodeless $1b_1$, is an in-phase combination of the $2p_\pi$ AO's on the pyrrole and benzo rings. The single-node orbitals $2b_1$ and $1a_2$ are largely localized on the benzo rings (60 and 70% respectively). They have e_x and e_y character on the pyrrole part respectively, and are stabilized by bonding admixture of C $2p_\pi$ on the benzo part. As for the e_x and e_y notation used for the pyrrolic orbitals, we refer to ref 19 for a detailed discussion. Here we simply recall that the pyrrolic ring can be viewed as a cyclopentadiene (Cp) ring perturbed by the N substitution (see Figure 4), and, according to the pertinent C_{5v} nomenclature, the pyrrolic π electron system is characterized by a lowest A_1 combination, followed by the E_1 set of orbitals, which are no longer degenerate, the "e_x" partner with amplitude on N (and on the C_β carbon atoms) being more stabilized than the "e_y" partner with N in its nodal plane and high amplitude on the C_α atoms. The E_2 orbitals finally are also split by the N perturbation, but less so than the E_1 set.

The next BzPy orbitals of Figure 3, the $3b_1$ and $2a_2$, have two vertical nodal surfaces. Their character in the pyrrolic part is almost unchanged compared to the Py e_x and e_y orbitals, the $2a_2$ having very large (62%) amplitude at the C_α position, the $3b_1$ having a nodal surface passing very close to the C_α. There is an additional nodal surface in these orbitals between the Py and the Bz parts accounting for the higher energy of these orbitals as compared to the "e_x" and "e_y" orbitals of Py. In fact they may be considered as antibonding combinations of the "e_x" and "e_y" orbitals of Py with Bz orbitals, the lower lying $2b_1$ and $1a_2$ being the Py-Bz bonding counterparts with high amplitude at the C_m and C_o carbons. We have therefore denoted in Figure 3 the $1a_2$ as "e_y^+" and $2a_2$ as "e_y^-" and the $2b_1$ and $3b_1$ as "e_x^+" and "e_x^-". The next higher pair of orbitals of BzPy, $4b_1$ and $3a_2$, have in the Py part a strong resemblance to the "$e_{x^2-y^2}$" and "e_{xy}" orbitals of Py.

The distinguishing feature of the "e_x" and "e_y" derived orbitals is the different amplitude on the C_α atoms to which the aza bridges will attach in the phthalocyaninato ring. As the orbital energy diagram for $(BzPy)_4$ of Figure 3 displays, the "e_y^-" derived set has the largest dispersion in $(BzPy)_4$ in virtue of the considerable C_α amplitude of the $2a_2$ BzPy orbital. The important consequence is that the "e_y^-" derived $2a_{1u}$ orbital is higher in energy than the "e_y" derived $1a_{1u}$ in the $(Py)_4$ cage (cf. Figure 3 in ref 19).

Coming to the interaction diagram for $(BzPy)_4$ interaction with $(N)_4$ displayed in Figure 3, the interaction pattern shows interesting differences with respect to the one with $(CH)_4$ displayed in Figure 10 of ref 19. Note that we take as electron

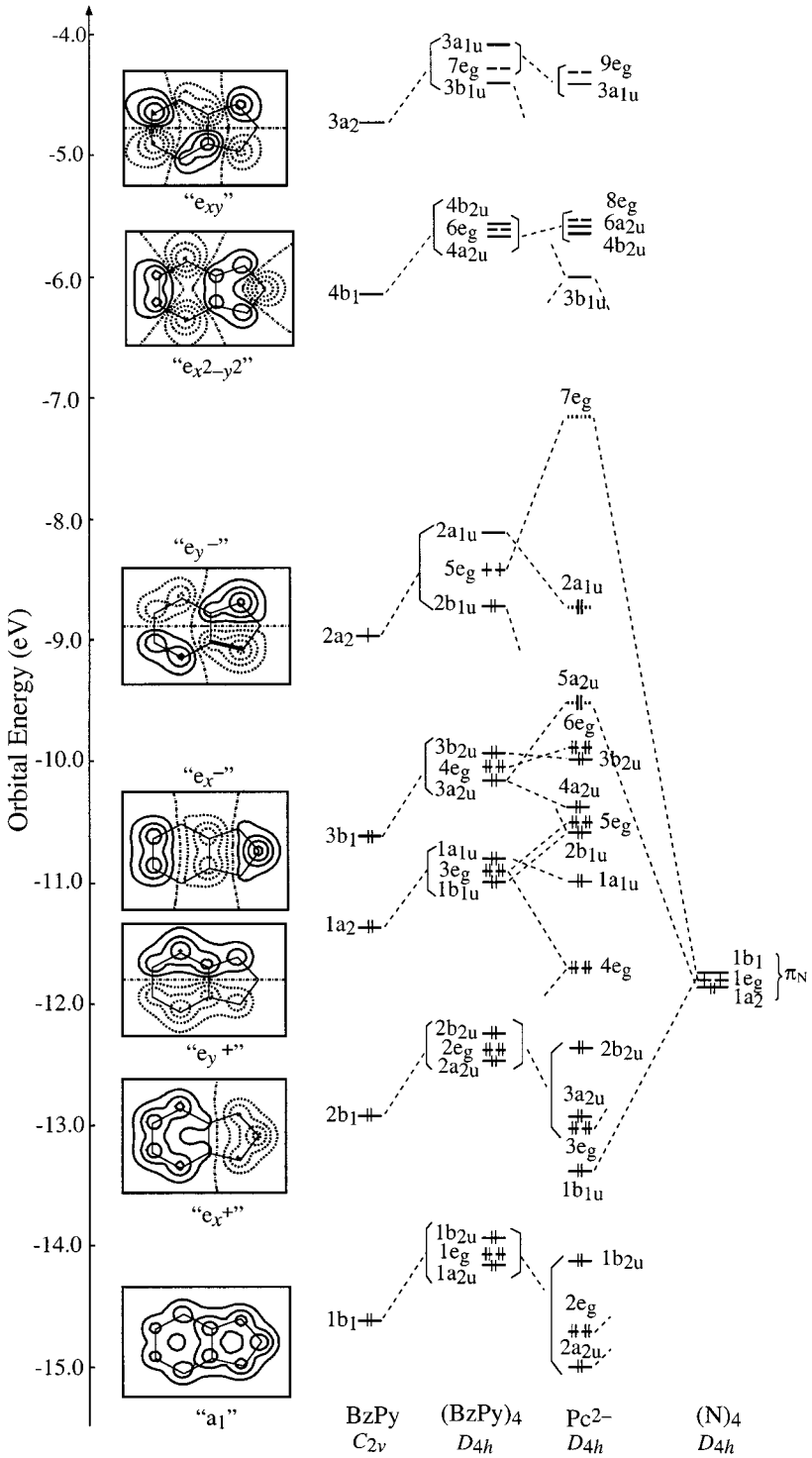

Figure 3. Orbital interaction diagram for interaction between the $(BzPy)_4$ cage and the four N bridges. Gouterman's four orbitals ($2a_{1u}$, $4a_{2u}$, $5e_{g,xz}$, and $5e_{g,yz}$) are indicated with hatched lines. The orbital numbering of the Pc ring system has been adapted to the situation in metal salt.

count for the $(BzPy)_4$ cage 38 electrons, the four times nine π electrons for the benzopyrrole rings being supplemented with two electrons in accordance with the -2 charge of the Pc ring in metal salts or with the two additional electrons coming from the in-plane hydrogen atoms in free base phthalocyanine. For ease of comparison with the ZnPc levels of Figure 2, we have adopted for the Pc levels of Figure 3 the same orbital numbers as in ZnPc, so the numbers of the a_{2u} and e_g orbitals of Pc have been raised by 1, to account for the presence of the Zn $3p_z$-a_{2u} and $3d_\pi$-e_g orbitals respectively below the π orbitals of Pc in the numbering of Figure 3.

An important difference between the aza and methine bridges is the higher electronegativity of the former resulting in an energetically lower lying set of $(N)_4$-p_π orbitals. Due to the lower energy of the $(N)_4$-p_π orbitals compared to the $(CH)_4$ set, the aza bridges will also interact to some extent with the low lying $(BzPy)_4$ orbitals of the $1b_1$ and $2b_1$ sets, causing stabilization of the $1b_1$-derived Pc $2a_{2u}$ and $2e_g$ orbitals and the $2b_1$ derived $3a_{2u}$ and $3e_g$ orbitals.

As a consequence of the stronger electronegativity (lower orbital energies) of (N_4) compared to $(CH)_4$ the final charge distribution is on $(N)_4$ more negative and on $(BzPy)_4$ more

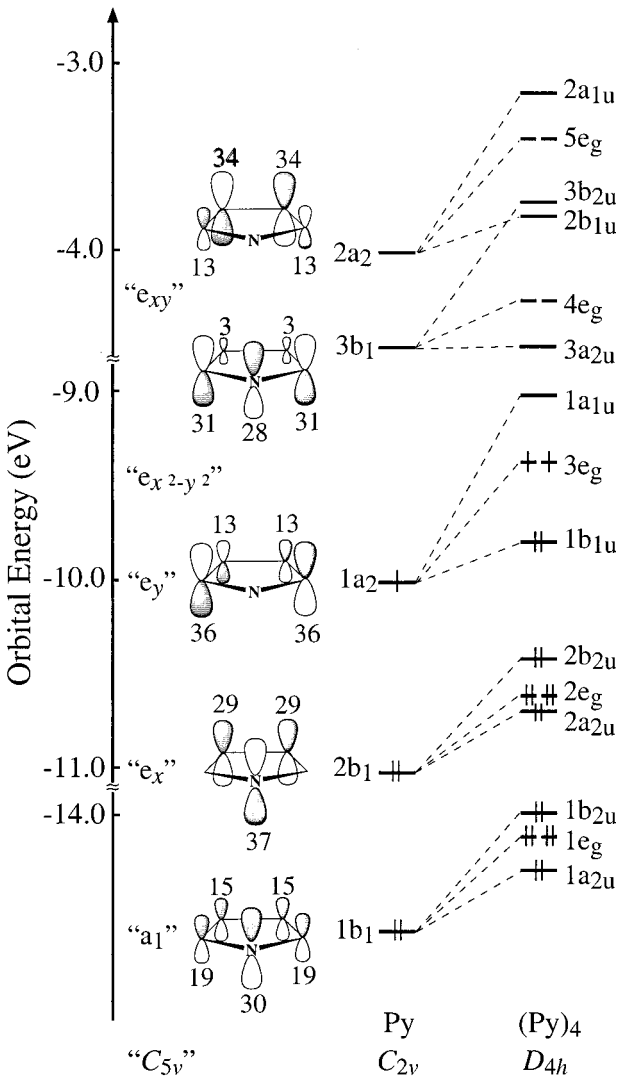

Figure 4. π Orbitals and orbital energies of the pyrrolic ring system. The contributions of the individual C p_z atomic orbitals to the MOs, in percentages based on Mulliken gross orbital populations per MO, are indicated in the figure. Orbital levels in the $(Py)_4$ cage are also given.

positive. This shows up in a general downward shift in energy of orbitals which do not interact strongly or even have a pure $(BzPy)_4$ character, such as the a_{1u} and b_{2u}-type orbitals. Nevertheless, the pure BzPy localized $2a_{1u}$ "G" orbital is still well above the other occupied π orbitals of the Pc ring and, just as in NiTBP and NiPc, is the HOMO.

As for the "G" $7e_g$ LUMOs, they arise from antibonding interaction of the $5e_g$-"e_y^-" of $(BzPy)_4$ with the $1e_g$ of the $(N)_4$ cage and are stabilized by interaction with the higher lying e_g orbitals of the $(BzPy)_4$ cage. The HOMO and LUMO are of course most important for the lowest absorption band (Q), see section 4.

Below the HOMO $2a_{1u}$, we find in Figure 3 a whole group of levels, derived from the e_x^- and e_y^+ BzPy levels, which are all (except for the $4e_g$) lying between -10 and -11 eV (see Figure 2) in Pc. The order of these levels can be understood from Figure 3, except for the "Gouterman" $5a_{2u}$. The next intense absorption band following the Q band will derive intensity from excitation to the LUMO $7e_g$ out of the "Gouterman" a_{2u} orbital which is included in the dense set of π levels between -10 and -11 eV, cf. Figure 2. In view of the importance of this orbital for the excitation spectrum we consider the position

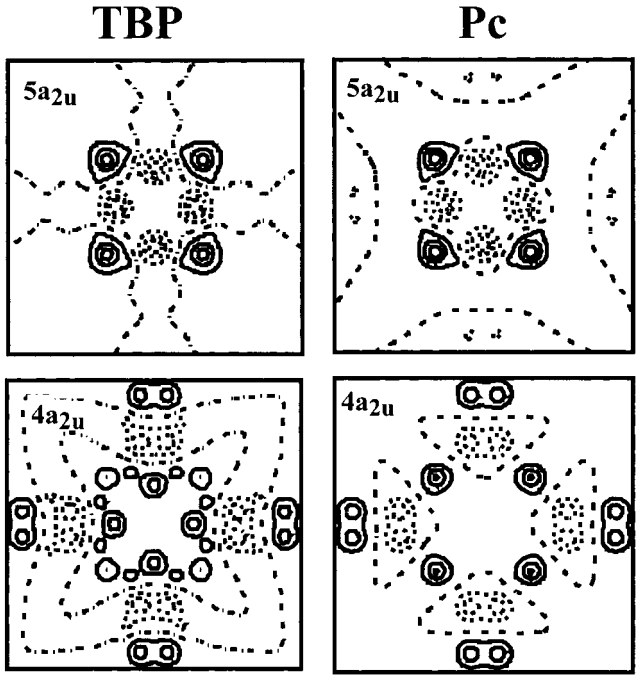

Figure 5. Contour plots of the $4a_{2u}$ and $5a_{2u}$ orbitals of Pc and TBP rings. The plane of drawing is 0.3 bohr above the molecular plane. Contour values are 0.0, $\pm$0.02, $\pm$0.05, $\pm$0.1, $\pm$0.2, $\pm$0.5 (e/bohr^3)$^{1/2}$.

of the Gouterman a_{2u} orbital in the orbital energy diagram in some detail below.

Inversion of "Gouterman"-Type a_{2u} and e_x^--Type a_{2u}. The difference in electronegativity between the aza and methine bridges has a major effect on the character of the two highest occupied a_{2u} orbitals, the $4a_{2u}$ and $5a_{2u}$. Unlike in TBP where the former is a nearly pure e_x^--derived $(BzPy)_4$-$3a_{2u}$ orbital and the latter is a $(CH)_4$-$1a_{2u}$ orbital with some admixture of the high lying $e_{x^2-y^2}$-type $(BzPy)_4$-$4a_{2u}$,[19] in Pc these $(BzPy)_4$ and bridge $(N)_4$ orbitals strongly interact, resulting in $4a_{2u}$ and $5a_{2u}$ orbitals which have mixed $(BzPy)_4$-$3a_{2u}$ and $(N)_4$-$1a_{2u}$ character. The percentages of these fragment orbitals are 36 and 34 in the $5a_{2u}$, and 64 and 18 in the $4a_{2u}$. The lower lying $1a_{2u}$ and $2a_{2u}$ and the higher lying $4a_{2u}$ orbitals of the $(BzPy)_4$ cage enter with only small contributions.

So, the character of the $5a_{2u}$ and $4a_{2u}$ changes on going from TBP to Pc. The mixing between $(BzPy)_4$-$3a_{2u}$ and $(N)_4$-$1a_{2u}$ is equivalent to a mixing of the TBP $5a_{2u}$ and $4a_{2u}$ to give the Pc $5a_{2u}$ and $4a_{2u}$. As inferred from the plots of these orbitals displayed in Figure 5, the $4a_{2u}$ of Pc is basically the $4a_{2u}$ of TBP with an admixture of the TBP-$5a_{2u}$, to the effect that almost all of the N_p character disappears and appreciable N_b character appears. The Pc "G"-$5a_{2u}$ is basically the "G"-$5a_{2u}$ of TBP with an "out-of-phase" admixture of TBP-$4a_{2u}$ resulting in an enhanced amplitude at the pyrrolic nitrogens and somewhat reduced amplitude at the bridging N_b atoms.

This change of character of the $4a_{2u}$ and $5a_{2u}$ orbitals has as an important consequence that the Pc-$5a_{2u}$, just because of its enhanced amplitude at the pyrrolic nitrogens, is so strongly stabilized by the metal $4p_z$ as to end up below the (original) $4a_{2u}$ in the metal salts. As is evident from the plots of the $5a_{2u}$ and $4a_{2u}$ of ZnPc and NiPc displayed in Figure 6, it is the lower lying $4a_{2u}$ that correlates with the "G"-$5a_{2u}$ of Pc and TBP. The $5a_{2u}$ of ZnPc and NiPc correlates with the lower lying $4a_{2u}$ of Pc and TBP. We note in passing that in NiTBP the downshift of the "G"-$5a_{2u}$ induced by the Ni-$4p_z$ is not so large as to cause reversal of the character of the two highest occupied a_{2u} orbitals of the ring system (cf. Figure 6 of ref 19).

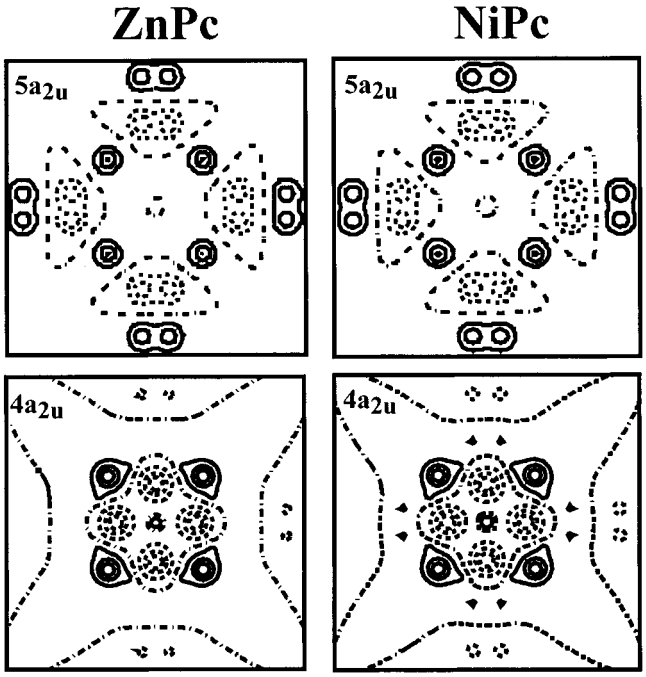

Figure 6. Contour plots of the $4a_{2u}$ and $5a_{2u}$ orbitals of NiPc and ZnPc. The plane of drawing is 0.3 bohr above the molecular plane. Contour values are 0.0, ±0.02, ±0.05, ±0.1, ±0.2, ±0.5 $(e/bohr^3)^{1/2}$.

It is worth noting that in ZnPc and even more in NiPc, the actual "G"-a_{2u} orbital, the $4a_{2u}$, is shifted very far down with respect to the "G"-$2a_{1u}$, due to the combined effect of upshift of the $2a_{1u}$ caused by the antibonding with the benzo rings (cf. Figure 3) and the downshift of the "G"-a_{2u} caused by the orbital mixing effects just discussed and the resulting interaction with $4p_z$ of the metal.

As a matter of fact the $4a_{2u}$ is so low as to come very close to the e_y^+ based $1a_{1u}$. The $4a_{2u}/1a_{1u}$ proximity is reminiscent of the a_{2u}/a_{1u} (near-)degeneracy in porphyrins and will receive special attention in the discussion of the excitation spectrum of ZnPc.

N_b and N_p Lone Pairs. In addition to the π levels, there are the in plane levels associated with N_p and N_b lone pairs, see left panel in Figure 2. In the D_{4h} symmetry of the molecule the four N_p lone pair combinations transform as b_{1g}, e_u, a_{1g}, and the four N_b lone pair combinations as b_{2g}, e_u, and a_{1g}.

The N_p related ZnPc orbitals are the $11b_{1g}$, $17e_u$, and $18e_u$ (the N_p lone pair e_u combinations get divided over these two orbitals) and the low lying $11a_{1g}$ (not reported in Figure 2). The N_p lone pairs of E_u and A_{1g} symmetry are stabilized by interaction with the $4p_\sigma$ and 4s Zn orbitals respectively (cf. the composition of the $11a_{1g}$, $17e_u$, and $18e_u$ reported in Table 2). In contrast, the N_p lone pair combination of B_{1g} symmetry, the $11b_{1g}$, is pushed up by antibonding with the Zn-$d_{x^2-y^2}$ (see ref 17 and cfr. the composition of this orbital in Table 2) and ends up just above the set of π orbitals in the right panel of Figure 2, but still well below the HOMO. The $11b_{1g}$ is actually the HOMO-1 of the molecule, but a large energy gap (~1.1 eV) separates this orbital from the HOMO.

Unlike the pyrrolic N lone pairs, the N_b lone pair orbitals $9b_{2g}$, $19e_u$, and $13a_{1g}$ are fairly close together. They point outward and are not particularly well suited for interactions with the metal that could increase the dispersion of this set. It is important, in view of the later discussion of the excitations out of these N_b lone pair orbitals, to note that they are lying well below the $2a_{1u}$ HOMO. Since the N_b lone pairs lie in the same energy region as the π orbitals associated with the B_1 and B_2 bands, i.e., the $5a_{2u}$, $4a_{2u}$, and $1a_{1u}$, the symmetry allowed $n\rightarrow\pi^*$ transitions are expected to contribute to the B band region rather than to the region slightly to the blue of the Q band. This is interesting since the possibility that an $n\rightarrow\pi^*$ transition occurs in this region has received considerable attention in the experimental work.[9,10,49] Actually, because of the large HOMO/HOMO-1 energy gap, we do not expect electronic transitions to occur in the high energy shadow of peak Q. We will quantify these statements in the discussion of the calculated spectrum in the next section.

Zn 3d Orbitals. As inferred from the energy and composition of the ZnPc MOs reported in Table 2, the Zn-3d shell remains almost unperturbed in the low energy region of the electronic spectrum, the only 3d orbital which interacts to some extent with the macrocycle being, as above-mentioned, the $d_{x^2-y^2}$.

Excited States and Optical Spectra

Q and B Band Region. The energies and oscillator strengths of the dipole allowed ^1E_u and $^1A_{2u}$ excited states of ZnPc through 4.0 eV are collected in Table 3 together with the experimental band maxima obtained from gas-phase,[12] room-temperature solution,[8] cryogenic temperature vitrified solution, [9] and argon matrix[10] spectra.

Q-Band. The excitation energy and oscillator strength of the 1^1E_u state leave no doubt on the assignment of this state to the intense Q band located at 1.88 eV (659 nm) in the gas-phase spectrum and at 1.85 eV (670 nm) in Ar/matrix,[10] room-temperature solution spectra[8] and cryogenic temperature vitrified solution[9] spectra of ZnPc. The (near)-degeneracy of the "G"-a_{1u} and a_{2u} orbitals which exists in porphyrins is lifted by the electronic effects of the aza bridges and benzo rings, hence the mixing of the $(a_{1u}e_g)$ and $(a_{2u}e_g)$ configurations and the consequent cancellation of the associated transition dipole moments occurring in the Q band of porphyrins does not occur in phthalocyanines. The 1^1E_u is indeed a nearly pure (92%) $2a_{1u}\rightarrow 7e_g$ state and its oscillator strength is almost entirely determined by the very large (4.17 au) transition dipole moment of the $2a_{1u}\rightarrow 7e_g$ transition.

B_1/B_2 Band Region. Before discussing the B_1/B_2 band region proper, we note that there have been suggestions in the literature that there is a very weak transition just to the red of the B_1 band, referred to as "2nd $\pi\rightarrow\pi^*$".[14,50,51] It was reported for MgPc at 2.85 eV (435 nm)[14,50] and suggested for ZnPc on the basis of ZINDO calculations.[51] We indeed find a transition just to the red of the B_1 band region, at precisely 2.87 eV. It is an almost pure $3b_{2u}\rightarrow 7e_g$ transition, the low intensity is in agreement with the e_x^- nature of the $3b_{2u}$ (cf. Figure 3 and section 3).

A considerable experimental effort has been spent to gain insight into the nature and number of excited states contributing to the B band. In the gas-phase spectrum reported by Edwards and Gouterman (see Figure 7),[12] the B band region is characterized by a broad intense and featureless absorption with the maximum located at 3.80 eV (326 nm). A split of the B band in B_1 and B_2 components was clearly distinguished by Nyokong et al.[8] in the absorption and MCD room-temperature solution spectra of ZnPc(L) (L = cyanide, imidazole, pyridine). These authors for the first time invoked MCD spectra as an aid in the deconvolution analysis. In the region of interest they required for the fitting of the MCD spectra the presence of two Faraday *A* terms, indicating that two degenerate excited states ("B_1 and B_2") exist in the B band region. In the case of zinc phthalocyanine with cyanide they were located at 3.21 eV (386 nm)

TABLE 3: Calculated Excitation Energies (eV) and Oscillator Strengths (*f*) for the Optically Allowed ^1E_u and $^1A_{2u}$ Excited States Contributing to the Q and B Band Region Are Compared to the Experimental Data. The Major One-Electron Transitions Contributing to SAOP/ALDA Solution Vectors Are Also Given

					exp.			
state	composition (%)	exc. en.	*f*	assignment	gas phase[a]	solution[b]	solution[c]	Ar matrix[d]
1^1E_u	92 ($2a_{1u}\rightarrow 7e_g$); 8 ($4a_{2u}\rightarrow 7e_g$)	1.96	0.7356	Q	1.88 (Q)	1.85 (Q)	1.85 (Q)	1.85 (Q)
2^1E_u	92 ($3b_{2u}\rightarrow 7e_g$)	2.87	0.0307	2nd $\pi\rightarrow\pi^*$				
3^1E_u	66 ($5a_{2u}\rightarrow 7e_g$); 16 ($2b_{1u}\rightarrow 7e_g$) 14 ($4a_{2u}\rightarrow 7e_g$)	3.07	0.0518				**3.05** (B_1)	3.05 (B_1 origin)
4^1E_u	73 ($2b_{1u}\rightarrow 7e_g$); 13 ($5a_{2u}\rightarrow 7e_g$) 6 ($4a_{2u}\rightarrow 7e_g$)	3.14	0.3032	B_1		3.21 (B_1)	3.17	
1^1A_{2u}	99 ($19e_u\rightarrow 7e_g$)	3.28	0.0011					
5^1E_u	88 ($2a_{1u}\rightarrow 8e_g$); 6 ($2b_{1u}\rightarrow 7e_g$)	3.34	0.0446				**3.30** (B_1)	
6^1E_u	47 ($1a_{1u}\rightarrow 7e_g$); 39 ($4a_{2u}\rightarrow 7e_g$) 8 ($5a_{2u}\rightarrow 7e_g$)	3.50	0.6572				**3.56** (B_2)	3.71 (B_2)
7^1E_u	47 ($1a_{1u}\rightarrow 7e_g$); 31 ($4a_{2u}\rightarrow 7e_g$) 8 ($5a_{2u}\rightarrow 7e_g$)	3.81	1.1548	B_2	3.80 (B)	3.75 (B_2)	**3.81** (B_2)	3.74 (B_1 max)
2^1A_{2u}	99 ($9b_{2g}\rightarrow 3b_{1u}$)	4.23	0.0012				4.05	3.99 (B_3)

[a] Data for ZnPc in gas-phase, from ref 12. [b] Data for (CN)ZnPc, in DMA solution, at room temperature, from ref 8. [c] Data for (CN)ZnPc, in solution, at cryogenic temperature, from ref 9, bold type is used for the Janh-Teller split components of the B_1 and B_2 bands. [d] Data for ZnPc in Ar/matrix, from ref 10.

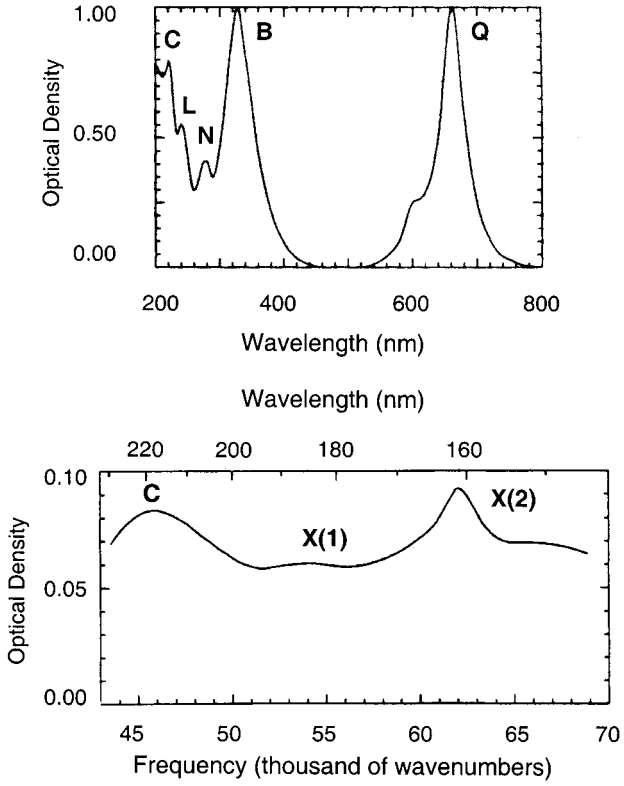

Figure 7. Gas-phase spectrum of ZnPc from ref 12. (Top) UV−vis region. (Bottom) Vacuum UV region.

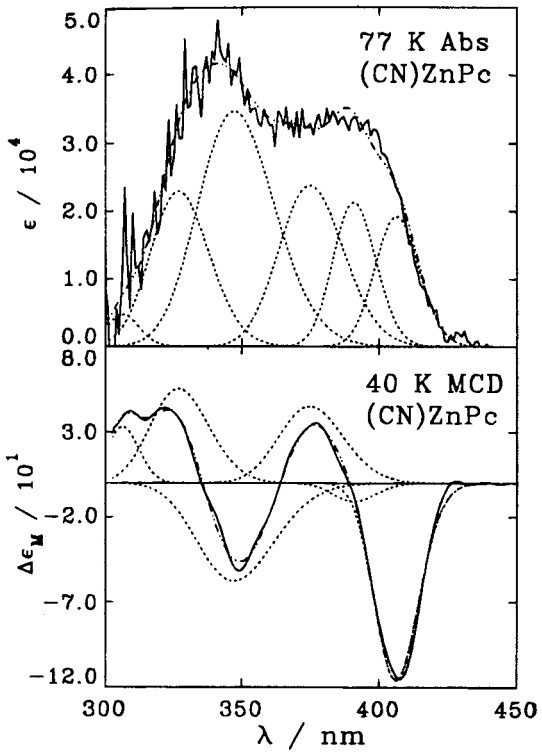

Figure 8. Deconvolution of the spectral bands in the B1/B2 region of (CN)ZnPc, from ref 9.

and 3.75 (331 nm), respectively. A second deconvolution analysis of the absorption and MCD spectra of ZnPc in Ar/matrix by VanCott et al.[10] also suggests (at least) two absorptions, with however different characteristics. They propose one very broad absorption band with a maximum at 3.74 eV (332 nm), which they call B_1. The onset of this band is identified as an observed origin at 3.05 eV (406 nm) which is followed by a progression of seven bands before the maximum at 3.74 eV. They believe that an experimental band maximum positioned at 3.71 eV (334 nm) does not fit into this pattern and corresponds to a separate electronic transition. On the basis of the MCD spectrum, they ascribe the strong broad band with maximum at 3.74 eV and the extra weaker band at 3.71 eV to two separate degenerate excited states and denote them as B_1 and B_2 respectively.

More recently, Mack and Stillman[9] have reported a band deconvolution analysis of the absorption and MCD spectral data of (CN)ZnPc recorded at cryogenic temperature. The UV absorption spectrum of the B band region published by these authors with the deconvolution into five underlying bands obtained from a simultaneous fit of their absorption and MCD spectra is reproduced in Figure 8. They found that in the B band region the MCD spectrum could not be properly fitted using two *A* terms, as had been done in the earlier work by Nyokong et al.[8] and VanCott et al.,[10] since a considerable residual intensity would have not been accounted for. A satisfactory fit was obtained replacing the *A* terms by two *B* terms of opposite sign with a slight separation (a pseudo-*A* term), which can be rationalized by a Jahn−Teller splitting of a degenerate state into two nondegenerate states which give rise to *B* terms. Mack and Stillman place the energy maxima of the

two Janh-Teller split components of the excited-state responsible for the B_1 band, which previously was assigned an energy of 3.21 eV, at 3.05 and 3.30 eV (406 and 375 nm), see Table 3 and Figure 8. Two more intense JT split components of the B_2 band, replacing the previous degenerate state at 3.75 eV are placed at 3.57 and 3.81 eV (348 and 325 nm) in the deconvolution analysis. Between the two oppositely signed *B* terms comprising the pseudo-*A* fit of the B_1 band, an additional Faraday *B* term at 3.17 eV (391 nm) was introduced in the fit.

As can be seen in Table 3, there is an excellent correspondence between the energies of the five bands of the deconvolution of Mack and Stillman and the five calculated ^1E_u transitions $3^1E_u-7^1E_u$ (we leave the $n\rightarrow\pi^*$ 1^1A_{2u} with very little intensity aside; see discussion of $n\rightarrow\pi^*$ bands below). The level of agreement, closer than 0.1 eV, must be fortuitous, although the calculations with the present method (TDDFT with SAOP Kohn−Sham potential) do attain that level of accuracy for the benchmark small molecules we have used to test the present theoretical method.[40,41] It is interesting to note the present agreement since this is a case where the experimental spectra have been carefully analyzed and much more detailed inferences about number, intensities and energies of the transitions have been made than is usually available from the broad experimental bands for large molecules. In comparing to our calculated results we note that the calculated intensities differ somewhat from the experimental ones. The $6,7^1E_u$ are the most intense ones, corresponding to the experimental higher intensity in the B_2 region, but we have the relative intensities of 6^1E_u and 7^1E_u reversed compared to the deconvolution of Figure 8. However, our intensities are not so quantitatively reliable, they are very sensitive to the density functional used and to basis set, geometry, etc. But it is also not clear whether a good fit of the experimental spectrum is not also possible with a higher intensity of 7^1E_u rather than 6^1E_u. The same holds for the three transitions in the B_1 region, $3,4,5^1E_u$. Maybe a good fit is also possible with high intensity for the 4^1E_u and weaker sidebands corresponding to 3^1E_u and 5^1E_u, as suggested by our calculations.

Despite the good agreement between calculated and experimental number and energy of the bands and a reasonable, or hopefully after refitting even good, agreement for intensities, there is a major discrepancy between the basis of our theoretical results, namely unsplit degenerate states, and the underlying assumptions of the fit to experiment, namely the JT splitting of the degenerate states so that only nondegenerate excited states remain. In view of the generally very high quality of the TDDFT results for this type of systems,[19,30,31] we consider it unlikely that our number of states in this region (five ^1E_u and one $^1A_{2u}$) is not correct. The calculated intensities do assign considerable intensity to the B_1 and B_2 regions and support this assumption. Since the calculation of JT splittings is beyond the present investigation, we cannot make an assessment of the basic assumption of the fitting procedure. We are also not able to judge whether the fitting of the MCD spectrum with *A* terms for the degenerate states, as our results would require, can be completely ruled out by the experimental data. It is clear however that, if JT splitting is significant, and experimentally visible in splitting of the bands, it will not be so large as to shift states out of the B region, so the fitting will then have to account for 10 nondegenerate, pairwise very close-lying, states.

We end this discussion of the B_1/B_2 region with a description of the electronic nature of the excited states. With respect to the B_1 region we note that the intense 4^1E_u is mainly (73%) described by the $2b_{1u}\rightarrow 7eg$ transition, the $5a_{2u}\rightarrow 7e_g$ and the $4a_{2u}\rightarrow 7e_g$ transitions contributing with a minor but not negligible weight. The phases of the mixing coefficients of these transitions are such that the transition dipole moments of the $2b_{1u}\rightarrow 7eg$ and $5a_{2u}\rightarrow 7e_g$ transitions (1.20 and 2.20 au, respectively) add up and the transition dipole moment of the $4a_{2u}\rightarrow 7e_g$ transition (1.47 au) subtracts, resulting in a quite large oscillator strength ($f = 0.3032$). The $2b_{1u}\rightarrow 7eg$ transition derives strength from the e_y^- character that is shared by the $2b_{1u}$ and $7e_g$ involved orbitals leading to on-site [on $(BzPy)_4$] "overlap". Note that the "G" $4a_{2u}$ has a considerably reduced transition dipole to $7e_g$, compared to the 3.25 au value in NiP, as a consequence of the orbital mixings discussed in the Ground State Electronic Structure Analysis, which have reduced its N_b content to 39% (cf. Table 2). The orbital mixings discussed in the Ground State Electronic Structure Analysis have left considerable N_b character in $5a_{2u}$, and the $5a_{2u}\rightarrow 7e_g$ transition dipole is quite large. Most important for the intensity of the 4^1E_u is however the reinforcement of the transition dipoles of the $2b_{1u}\rightarrow 7e_g$ and $5a_{2u}\rightarrow 7e_g$. The 3^1E_u consists of the same orbital transitions as the 4^1E_u but has much lower intensity due to the cancellation of the transition dipoles.

With respect to the B_2 region, we note that predominantly the $4a_{2u}\rightarrow 7e_g$ (Gouterman type) and $1a_{1u}\rightarrow 7e_g$ transitions enter, in both the 6^1E_u and 7^1E_u. Due to the downshifting effect of the aza bridges and of the Zn-$4p_z$, the "G" $4a_{2u}$ is so low in ZnPc as to come very close to the "e_y^+" based $1a_{1u}$ (see Figure 2). This $4a_{2u}/1a_{1u}$ (bridge/e_y^+) near-degeneracy is reminiscent of the well-known (near-)degeneracy of the highest occupied "G" orbitals of a_{2u}/a_{1u} (bridge/e_y) character in porphyrins and causes the $4a_{2u}\rightarrow 7eg$ and the $1a_{1u}\rightarrow 7eg$ transitions to undergo, just as the $a_{2u}\rightarrow e_g$ and $1a_{1u}\rightarrow 5e_g$ do in metalporphyrin, a configuration mixing resulting in the 6^1E_u and 7^1E_u excited states. The transition dipole moments of the $4a_{2u}\rightarrow 7e_g$ and $1a_{1u}\rightarrow 7e_g$ transitions are however quite different, the transition dipole moment of the $4a_{2u}\rightarrow 7e_g$, although reduced from the typical "G" value in porphyrins (see above), is far larger than that of the $1a_{1u}\rightarrow 7e_g$ (1.47 vs 0.12 au). As a result, the oscillator strength of the lower lying combination where they have opposite direction is not almost zero as in the case of the Q state of porphyrins, but it is half that of the higher lying combination where they have parallel direction. The oscillator strengths of the 6^1E_u and 7^1E_u excited states are indeed both very large amounting to 0.6572 and 1.1548, respectively.

B_3 Band and the Issue of the $n\rightarrow\pi^*$ Transitions. In this section, we will address the still debated question of the location of the *n* (N_b lone pairs)$\rightarrow\pi^*$ transitions. Our electronic structure calculations, which locate the set of N_b lone pairs well below the HOMO, already suggest that the lowest allowed $n\rightarrow\pi^*$ transitions should lie in the B band region. Explicit calculations of the A_{2u} excited states confirm this suggestion. The lowest *z*-polarized $n\rightarrow\pi^*$ excited states, the 1^1A_{2u} which is dominated by the $19e_u$ (N_b lone pairs)$\rightarrow$ $7e_g$ (LUMO) transition, and the 2^1A_{2u} which is a nearly pure $9b_{2g}$ (N_b lone pair)$\rightarrow$ $3b_{1u}$ (π^*) state, are indeed computed at 3.28 and 4.23 eV, respectively. The theoretical prediction of the $n\rightarrow\pi^*$ 2^1A_{2u} state at 4.23 eV (293 nm) is perfectly in line with the experimental findings. Ar/matrix experiments by VanCott et al.[10] locate indeed a A_{2u} *z*-polarized $n\rightarrow\pi^*$ band labeled B_3 to the blue of the B band main peak (B_2), at 3.99 eV (310 nm). Nyokong et al.[8] also observed in their solution spectra of ZnPc with cyanide and imidazole ligands a band in the vicinity of the B_3 absorption (at 4.13 eV for cyanide and 3.96 eV for imidazole), showing pure Faraday *B* term. A weak band at 4.05 eV (306 nm) corresponding to a pure *B* term is also present in the deconvolution analysis of the B band performed by Mack and Stillman,[9]

TABLE 4: Calculated Excitation Energies (eV) and Oscillator Strengths (*f*) for the Optically Allowed ^1E_u and $^1A_{2u}$ Excited States Contributing to the N, L, and C Band Region Compared to the Experimental Data. The Major One-Electron Transitions Contributing to SAOP/ALDA Solution Vectors Are Also Given

					exp.		
state	composition (%)	exc. en.	*f*	assignment	gas phase[a]	solution[b]	Ar matrix[c]
3^1A_{2u}	99 ($11b_{1g}\rightarrow 4b_{2u}$)	4.31	0.0001				
8^1E_u	94 ($6e_g\rightarrow 3b_{1u}$)	4.32	0.0281				
9^1E_u	71 ($6e_g\rightarrow 4b_{2u}$); 16 ($3b_{2u}\rightarrow 8e_g$)	4.50	0.0054				
10^1E_u	58 ($5e_g\rightarrow 3b_{1u}$); 27 ($2a_{1u}\rightarrow 9e_g$)	4.50	0.0243				
11^1E_u	68 ($6e_g\rightarrow 6a_{2u}$); 20 ($3b_{2u}\rightarrow 8e_g$)	4.58	0.0374				
12^1E_u	45 ($2a_{1u}\rightarrow 9e_g$); 36 ($3b_{2u}\rightarrow 8e_g$)	4.64	0.0505				
13^1E_u	66 ($5e_g\rightarrow 4b_{2u}$); 23 ($5e_g\rightarrow 6a_{2u}$)	4.69	0.0150				
14^1E_u	62 ($5a_{2u}\rightarrow 8e_g$); 18 ($3b_{2u}\rightarrow 8e_g$)	4.77	0.1402	N	4.49 (N)	4.52 (N)	4.41 (N_1)
4^1A_{2u}	98 ($18e_u\rightarrow 7e_g$)	4.78	~0				
15^1E_u	48 ($5e_g\rightarrow 6a_{2u}$); 45 ($2b_{1u}\rightarrow 8e_g$)	4.81	0.0003				4.70 (N_2)
16^1E_u	85 ($4a_{2u}\rightarrow 8e_g$)	4.98	0.0200				4.88 (L_1)
5^1A_{2u}	96 ($19e_u\rightarrow 8e_g$)	5.05	0.0016				
6^1A_{2u}	95 ($17e_u\rightarrow 7e_g$)	5.09	0.0001				
17^1E_u	33 ($1a_{1u}\rightarrow 8e_g$); 28 ($2b_{1u}\rightarrow 8e_g$);	5.13	0.0679	L	5.17 (L)		5.09 (L_2)
18^1E_u	88 ($2b_{2u}\rightarrow 7e_g$)	5.28	0.0007				5.33 (L_3)
7^1A_{2u}	100 ($16e_u\rightarrow 7e_g$)	5.50	0.0002				
19^1E_u	15 ($4a_{2u}\rightarrow 8e_g$); 11 ($3b_{2u}\rightarrow 8e_g$); 10 ($6e_g\rightarrow 4b_{2u}$); 10 ($6e_g\rightarrow 6a_{2u}$)	5.50	1.5942	C	5.63 (C)		5.62 (C_1)
8^1A_{2u}	100 ($13a_{1g}\rightarrow 6a_{2u}$)	5.57	0.0011				
20^1E_u	81 ($3a_{2u}\rightarrow 7e_g$); 11 ($1a_{1u}\rightarrow 8e_g$)	5.60	0.0315				
21^1E_u	32 ($1a_{1u}\rightarrow 8e_g$); 13 ($2b_{1u}\rightarrow 8e_g$); 11 ($3a_{2u}\rightarrow 7e_g$); 9 ($5e_g\rightarrow 6a_{2u}$)	5.80	0.1800				5.92 (C_2)
:	:	:	:	:	:	:	:
26^1E_u	74 ($4a_{2u}\rightarrow 9e_g$); 12 ($2b_{1u}\rightarrow 9e_g$);	6.23	0.1800				5.99 (C_3)

[a] Data for ZnPc in gas-phase, from ref 12. [b] Data for (CN)ZnPc, in DMA solution, at room temperature, from ref 8. [c] Data for ZnPc in Ar/matrix, from ref 10

although these authors could not distiguish whether this band was vibrational or electronic in origin. We note that the energy and intensity of this band fit very well with the energy and the oscillator strength calculated for the 2^1A_{2u} state that is indeed very low ($f = 0.0012$), in virtue of the $\langle 9b_{2g}|z|b_{1u}\rangle$ transition dipole moment being, as expected for a $\sigma\rightarrow\pi^*$ transition, quite small (0.20 au).

As for the lowest $n\rightarrow\pi^*$ A_{2u} state, the 1^1A_{2u}, there is a clear disagreement about the location of this state between theory and suggestions made on the basis of Ar/matrix and cryogenic temperature vitrified solution experiments. Analysis of Shpol'ski matrix data by Huang et al.[49] and of Ar/matrix data by VanCott et al.[10] suggested the presence of an additional $n\rightarrow\pi^*$ electronic transition at 2.08 eV, in the "Q_{02}" region of the spectrum of ZnPc. This band was called Q′ and assigned to the e_u (N_b lone pairs) $\rightarrow$ e_g (LUMO) transition. On the basis of a deconvolution analysis of the absorption and MCD spectral data of a vitrified solution of (CN)ZnPc, Mack and Stillman[9] have recently supported this additional *z*-polarized electronic band centered at 2.05 eV (604 nm) in the so-called "Q_{02}" region, and also assigned this band to the e_u (N_b lone pairs) $\rightarrow$ e_g (LUMO) transition.

According to our calculations the lowest *z*-polarized state, the 1^1A_{2u}, which is dominated by the $19e_u$ (N_b lone pairs) $\rightarrow$ $7e_g$ (LUMO) $n\rightarrow\pi^*$ transition, lies at 3.28 eV, more than 1.1 eV higher than suggested by these experiments. Such a large error is unlikely, however, for TDDFT excitation energies. The energy we predict for the lowest $n\rightarrow\pi^*$ 1^1A_{2u} state closely agrees with previous results[13,51,52] by completely independent, although much less accurate, theoretical approaches. We also note that the second $n\rightarrow\pi^*$ excited state 2^1A_{2u} at 4.23 eV beautifully agrees with experiment.

In the energy regime of the "Q_{02}" band, we actually do not find any allowed excited state, the lowest dipole allowed excited state following the Q-band, the *x*,*y*-polarized $\pi\rightarrow\pi^*$ 2^1E_u state being calculated at 2.87 eV. Our prediction that a wide energy gap separates the Q state (S_1) from higher singlet excited states seems to agree with the results of recent spectroscopic studies by Rückmann et al.[53] on $ZnPc(OEt)_8$ (OEt = α-alkyloxy). These authors have observed indeed an anomalous luminescence band from a higher than S_1 excited state, at 2.8 eV, a feature that gives a hint for a large separation between the S_1 and higher singlet excited states. We note by the way that the 2.87 eV energy value we predict for the lowest singlet excited state above the S_1 state of ZnPc and we assign to the second $\pi\rightarrow\pi^*$ transition located by Mack et al.[51] to the red of B_1 band is close to the maximum of this fluorescence band. Thus, our theoretical results, in agreement with the fluorescence experiments, suggest that the band located in the "Q_{02}" region of the spectrum of ZnPc in Ar/matrix[10] and cryogenic temperature solution[9] experiments, does not have an electronic origin.

N, L, and C Bands. In the relatively narrow (~1.1 eV) energy range spanned by the N, L, and C bands (see Figure 7), our calculations (Table 4) predict a considerable number of closely spaced E_u excited states. As inferred from their composition, these states arise from $\pi\rightarrow\pi^*$ transitions connecting the e_x^- and e_y^+ based MO levels together with the $2b_{1u}$ (e_y^- based) MO level which are very crowded in the −10 to −11 eV region (see Figures 2 and 3) to low lying π^* levels, such as the purely BzPy $4b_{2u}$, $6a_{2u}$, $8e_g$, and the $3b_{1u}$ of mixed BzPy-e_{xy} and bridge-$1b_{1u}$ character. All these transitions have a rather low dipole moment since they connect MOs which derive from different fragment orbitals at the BzPy side and/or at the N_4 side (cf. the interaction diagram of Figure 3) and hence have small on-site overlap. As a matter of fact, except for the C band where a constructive interference of transitions with relatively low dipole moments occurs (see below), we calculate little intensity in this region.

This is in agreement with both gas-phase[12] and Ar/matrix[10] spectra showing in the C band region the strongest absorption outside the B band region and in the N and L region bands, which are relatively weak in comparison with the B band.

TABLE 5: Calculated Excitation Energies (eV) and Oscillator Strengths (*f*) for the Optically Allowed ^1E_u and $^1A_{2u}$ Excited States Contributing to the Band Region Are Compared to the Experimental Data. The Major One-Electron Transitions Contributing to SAOP/ALDA Solution Vectors Are Also Given

					exp.		
state	composition (%)	exc. en.	*f*	assignment	gas phase[a]	Ar matrix[b]	thin film[c]
39^1E_u	35 ($6e_g \rightarrow 7a_{2u}$); 35 ($5e_g \rightarrow 4b_{1u}$); 12 ($2b_{2u} \rightarrow 8e_g$)	6.95	0.4586	X_1	6.89 (X_1)	6.89 (X_1)	6.94(X_1)
40^1E_u	18 ($2b_{2u} \rightarrow 8e_g$); 16 ($1b_{2u} \rightarrow 7e_g$) 12 ($5e_g \rightarrow 7a_{2u}$); 10 ($6e_g \rightarrow 4b_{1u}$)	6.99	0.4172				
48^1E_u	35 ($11b_{1g} \rightarrow 21e_u$); 21 ($3e_g \rightarrow 6a_{2u}$); 13 ($19e_u \rightarrow 12b_{1g}$); 10 ($5e_g \rightarrow 7a_{2u}$)	7.33	0.4608	X_2	7.75 (X_2)	7.67 (X_2)	7.69 (X_2)
50^1E_u	32 ($3e_g \rightarrow 6a_{2u}$); 17 ($5e_g \rightarrow 7a_{2u}$)	7.41	0.4410				
51^1E_u	97 ($9b_{2g} \rightarrow 21_{eu}$)	7.47	0.1717				
29^1A_{2u}	61 ($2b_{1u} \rightarrow 10b_{2g}$); 39 ($6e_g \rightarrow 21e_u$)	7.50	0.0171				
52^1E_u	92 ($19e_u \rightarrow 10b_{2g}$)	7.67	0.1137				
30^1A_{2u}	100 ($5e_g \rightarrow 21e_u$)	7.71	0.0256				
54^1E_u	97 ($13a_{1g} \rightarrow 20e_u$)	7.82	0.1264				

[a] Data for ZnPc in gas-phase, from ref 12. [b] Data for ZnPc in Ar/matrix, from ref 10. [c] Data for ZnPc in thin film, from Ref 7.

The strongest excited-state we predict in the N band region is the 14^1E_u calculated at 4.77 eV and with oscillator strength of 0.1402. Comparison with the experimental band maxima of 4.49, 4.52, and 4.41 eV obtained from gas-phase,[12] solution,[8] and Ar/matrix[10] spectra, respectively, suggests that our calculations slightly overestimate the energy of the N band. It should be noted however that the 14^1E_u state which is dominated by the transition from the e_y^--$5a_{2u}$ to the $e_{x^2-y^2}-8e_g$ and which we assign to the N band, contributes only 50% to the intensity of this band, the remaining 50% coming from the four close lying ^1E_u excited states just below the 14^1E_u, i.e., the 10^1E_u, 11^1E_u, 12^1E_u, and 13^1E_u calculated at 4.50, 4.58, 4.64, and 4.69 eV, respectively, for which we find a summed oscillator strength of 0.1272, that puts our results more in line with the experiment.

Ar/matrix experiments by VanCott et al.[10] identify a second, much weaker N band labeled N_2 at 4.70 eV. According to their MCD data, this band originates from an electronic transition of the type $^1A_{1g} \rightarrow {}^1E_u$. We associate the N_2 band to the very weak 15^1E_u state calculated at 4.81 eV.

In the L band region, we predict only two ^1E_u states of appreciable intensity, the 16^1E_u and 17^1E_u. The latter calculated at 5.13 eV (242 nm) and with oscillator strength of 0.0679 nicely accounts for the experimental L band maximum of 5.17 eV (240 nm) and 5.09 eV (244 nm) (L_2) observed in gas-phase[12] and Ar/matrix[10] spectra, respectively. The 16^1E_u calculated at 4.98 eV (249 nm) and with oscillator strength of 0.0200 could be correlated to the L_1 band identified at 4.88 eV (249 nm) by VanCott et al.[10] in Ar/matrix absorption and MCD spectra to the red of the L_2 band. These authors identified also a third very weak L band, L_3, to the blue of the L band main peak, at 5.33 eV (233 nm) corresponding to a negative Faraday *A* (or pseudo-*A*) term in the MCD spectra and hence arising from an electronic transition of the type $^1A_{1g} \rightarrow {}^1E_u$. The very weak ^1E_u state, the 18^1E_u, we predict at 5.28 eV (235 nm) could well account for the L_3 band.

According to our calculations, the 19^1E_u excited state at 5.50 eV (225 nm) is responsible for the C band centered in the gas-phase spectrum of ZnPc at 5.63 eV (220 nm). The large (1.5942) oscillator strength of this state fits in with the C band being the strongest outside the B band region. As inferred from its composition, the 19^1E_u shows a high degree of configuration mixing, the transition with the largest weight contributing by only 15% to the composition of this state. As above-mentioned, although the individual transitions contributing to the 19^1E_u have relatively small dipole moments, the phases of the mixing coefficients are such that the individual transition dipole moments interfere constructively resulting in a large oscillator strength.

Ar/matrix studies[10] locate three bands corresponding to transitions of the type $^1A_{1g} \rightarrow {}^1E_u$ in the C region, C_1 at 5.62 eV (221 nm), C_2 at 5.92 eV (209 nm), and C_3 at 5.99 eV (207 nm).

The excitation energy values of 5.50, 5.80, and 6.23 eV (225, 214, and 199 nm) we predict for the three most intense E_u states belonging to the C band region, the $19E_u$, $21E_u$, and $26E_u$, are in nice agreement with the C_1, C_2, and C_3 experimental band maxima. The calculated and the observed intensities of these bands do not agree as well as the energies, however. The intensity distribution observed for the C bands follows indeed the order $C_3 > C_1 \gg C_2$, at variance with our calculations which predict the C_1 ($19E_u$) state at 5.50 eV as the most intense. This discrepancy seems, however, to be due to matrix effects rather than to a failure of the calculations, as suggested by the excellent accord between our results and gas-phase spectrum of ZnPc showing the C band maximum at 5.63 eV.

As inferred from Table 4, in the region of the N, L, and C bands, we find several $^1A_{2u}$ excited states. They all have very small oscillator strength and hence contribute little to the intensity of this spectral region. The composition of the $^1A_{2u}$ states listed in Table 4 indicates that they are single transition states involving excitations from N_b and N_p lone pair orbitals, such as the $13a_{1g}$, $19e_u$, $11b_{1g}$, $18e_u$, and $17e_u$, to the LUMO or to the BzPy π orbitals of the $e_{x^2-y^2}$ set.

X Band Region. Gas-phase,[12] Ar/matrix,[10] and thin film[7] absorption spectra of ZnPc extending to the X bands of the vacuum ultraviolet region show an approximately constant absorption across the spectrum with two more intense bands, X_1 and X_2, centered at 6.89 and 7.75 eV (180 and 160 nm) in the gas-phase spectrum (see Figure 7), 6.89 and 7.67 eV (180 and 162 nm) in the Ar/matrix spectrum, 6.94 and 7.69 eV (179 and 161 nm) in the thin film spectrum. These experimental data are gathered in Table 5 together with the theoretical excitation energies and oscillator strengths of the allowed E_u and A_{2u} states with largest oscillator strength. Our calculations nicely describe this part of the vacuum ultraviolet region. Immediately to the blue of the C band and up to 8.0 eV, we compute indeed a plethora of excited states with low but not negligible intensity, accounting for the nearly constant absorption across the spectrum, and two pairs of nearly degenerate E_u states, the $39E_u$/$40E_u$ at 6.95 and 6.99 eV respectively, and the $48E_u$/$50E_u$ at 7.33 and 7.41 eV, respectively, with large and comparable

TABLE 6: Excitation Energies (eV) and Composition of the Lowest E_u and A_{2u} Triplet States

state	composition (%)	exc. en.	experiment
$1\ ^3E_u$	100 ($2a_{1u}\rightarrow 7e_g$)	1.27	1.13,[a] 1.14[b]
$2\ ^3E_u$	96 ($3b_{2u}\rightarrow 7e_g$)	2.71	
$3\ ^3E_u$	93 ($5a_{2u}\rightarrow 7e_g$)	2.89	
$4\ ^3E_u$	79 ($2b_{1u}\rightarrow 7e_g$); 17 ($4a_{2u}\rightarrow 7e_g$)	2.99	
$5\ ^3E_u$	80 ($4a_{2u}\rightarrow 7e_g$); 18 ($2b_{1u}\rightarrow 7e_g$)	3.03	
$1\ ^3A_{2u}$	100 ($19e_u\rightarrow 7e_g$)	3.11	

[a] Phosphorescence sectrum of ZnPc in chloronaphthalene at 77 K, from ref 54. [b] Phosphorescence spectrum of ZnPc in chloronaphthalene at 2 K, from ref 54.

oscillator strength, accounting for the X_1 and X_2 peaks. As inferred from their composition, the excited states responsible for the X_1 and X_2 peaks show a high degree of configuration mixing and involve also transitions to very diffuse outer orbitals, such as the Zn-4p_z based $7a_{2u}$, and the H-2s based $21e_u$ and $12b_{1g}$ orbitals. This fits in with the suggestion by VanCott et al.[10] that some of the transitions in the vacuum-UV involve excitations to Rydberg states. They observed indeed a considerable sharpening of the X_2 band on going from condensed phase (matrix and thin-film) to gas-phase absorption spectrum and a slight blue shift of this band on condensation, a behavior to be expected for a Rydberg transition.

Triplet Excited States. In view of the relevance of triplet excited states for the photochemical and photophysical properties of phthalocyanines, the lowest triplet states of E_u and A_{2u} symmetry have also been studied. The results are collected in Table 6 together with the experimental data coming from the phosphorescence spectra. The lowest triplet state of ZnPc is found to be the 1^3E_u state for which we compute a vertical excitation energy ($S_0\rightarrow T_1$) of 1.27 eV, in agreement with the energy 1.13−1.14 eV determined from the phosphorescence spectra in chloronaphthalene glass upon excitation in the Q band.[54] A large energy gap (1.44 eV) separates this state from a set of closely spaced ^3E_u states, the 2^3E_u, 3^3E_u, 4^3E_u, and 5^3E_u, which are located just below the lowest triplet of A_{2u} symmetry computed at 3.11 eV. In the triplet−triplet absorption spectrum of ZnPc$(OEt)_8$, Rückmann et al.[53] observed a broad, intense induced T_1-T_n absorption band in the region between 1.9 and 2.3 eV. Taking into account the energetic position of the T_1 state known from their phosphorescence studies (1.08 eV), these authors quote the energies of the relevant higher triplet states between 2.94 and 3.34 eV in ZnPc$(OEt)_8$. This is consistent with our results on ZnPc which indicate that the higher triplet states are located in the range 2.71−3.11 eV.

Conclusions

An accurate description of the UV−vis and vacuum−UV spectra of ZnPc has been provided by time-dependent density functional calculations of the excited states of this molecule. The theoretical results are in excellent agreement with gas-phase spectra and generally in line with deconvolution analyses of solution and Ar/matrix absorption and MCD spectra. The nature and intensity of the main spectral features have been highlighted and interpreted on the basis of the ground state electronic structure of the complex. A fragment approach where the four benzopyrrole rings and the aza bridges are taken as building blocks has proven to be a very important tool to fully understand the energy and composition of the MOs involved in the transitions. In particular, the different energy and character of the two highest occupied a_{2u} orbitals in tetrabenzoporphyrins and phthalocyanines has been explained and the actual "G"-a_{2u} orbital unambiguously identified.

The relevant results may be summarized as follows.

(i) The breakdown of the (near-)degeneracy of the a_{1u} and a_{2u} Gouterman orbitals known to exist in porphyrins causes the mixing between the ($a_{1u}e_g$) and ($a_{2u}e_g$) configurations occurring in porphyrins to almost vanish in phthalocyanines. The cancellation of transition dipoles that occurs in the low energy combination of these configurations in porphyrins, leading to very low intensity of the Q band, does not occur in phthalocyanines. The oscillator strength of the 1^1E_u (Q) state of ZnPc is indeed entirely determined by the large (4.17 au) transition dipole moment of the $2a_{1u}\rightarrow 7e_g$ transition. A wide energy gap (1.1 eV) is predicted between the Q state and higher singlet allowed excited states, in agreement with luminescence studies by Rückmann et al.[53] We are thus not able to identify an electronic origin for the band located ∼0.15 eV to the blue of the Q band, in the "Q_{02}" region, in solution and Ar/matrix absorption and MCD spectra. The lowest *z*-polarized $n\rightarrow\pi^*$ transition which has been suggested to be the source of this band is found in our calculations in the B band region. The other $n\rightarrow\pi^*$ transition, the $9b_{2g}$ (N_b lone pair) $\rightarrow$ $3b_{1u}$ (π^*) $^1A_{2u}$ state is computed just to the blue of the B band main peak, in perfect agreement with the experimental assignment.

(ii) The actual Gouterman orbital, the $4a_{2u}$, is so low in phthalocyanines as to come very close to the "e_y^+" based $1a_{1u}$ causing a configuration mixing of the Gouterman configuration ($4a_{2u}7e_g$) with the non-Gouterman ($1a_{1u}7e_g$) configuration. The resulting close lying and intense 6^1E_u and 7^1E_u excited states are responsible for the B band main peak (B_2). The close proximity of the higher lying a_{2u} orbital, the $5a_{2u}$, with the $2b_{1u}$ causes, in turn, the ($5a_{2u}7e_g$) and the ($2b_{1u}7e_g$) configurations to mix considerably in the weak 3^1E_u and in the relatively intense 4^1E_u excited state, the latter accounting for the shoulder (B_1) to the red of the B band main peak.

(iii) In the relatively narrow (∼1.1 eV) energy range spanned by the N, L, and C bands, a considerable number of closely spaced E_u excited states is predicted. The involved transitions have a rather low dipole moment since they connect MOs which derive from different fragment orbitals at the BzPy side and/or at the $(N)_4$ and hence have small on-site overlap. Thus, except for the C band where a constructive interference of transitions with relatively low dipole moments occurs, we calculate little intensity in this region, in agreement with gas-phase and Ar/matrix spectra showing in the C band region the strongest absorption outside the B band region and in the N and L region bands, which are relatively weak in comparison with the B band.

(iv) The main features of the vacuum ultraviolet region, showing an approximately constant absorption across the spectrum with two more intense bands, X_1 and X_2, are nicely described by our calculations which predict in this region a plethora of excited states with low but not negligible intensity and two pairs of nearly degenerate E_u states, with large and comparable oscillator strength.

(v) The predicted level pattern of the lowest triplet excited states fits in with phosphorescence data available and excited-state absorption spectra.

Acknowledgment. This research work was partially supported by the Italian MURST (Ministero dell′ Università e della Ricerca Scientifica) and the Università della Basilicata, Italy (GRANT 9903263473_005). We are also grateful to the National Computing Facilities foundation (NCF) of The Netherlands foundation for Scientific Research (NWO) for a grant of computer time.

References and Notes

(1) Wagner, R. W.; Lindsey, J. S.; Seth, J.; Palaniappan, V.; Bocian, D. F. *J. Am. Chem. Soc.* **1996**, *118*, 3996.

(2) Reimers, J. R.; Lü, T. X.; Crossley, M. J.; Hush, N. S. *Chem. Phys. Lett.* **1996**, *256*, 353.

(3) Leznoff, C. C.; Lever, A. B. P., Eds. *Phthalocyanines: Properties and Applications*; VCH Publishers: New York, 1990−1996; Vol. 1−4.

(4) Fernández, D. A.; Awruch, J.; Dicelio, L. E. *J. Photochem. Photobiol.* **1996**, *63*, 784.

(5) Lawrence, D. S.; Whitten, D. G. *Photochem. Photobiol.* **1996**, *64*, 923.

(6) Edwards, L.; Dolphin, D. H.; Gouterman, M. *J. Mol. Spectrosc.* **1970**, *35*, 90.

(7) Schechtman, B. H.; Spicer, E. W. *J. Mol. Spectrosc.* **1970**, *33*, 28.

(8) Nyokong, T. N.; Gasyna, Z.; Stillman, M. J. *Inorg. Chem.* **1987**, *26*, 1087.

(9) Mack, J.; Stillman, M. J. *J. Phys. Chem.* **1995**, *99*, 7935.

(10) VanCott, T. C.; Rose, J. L.; Misener, G. C.; Williamson, B. E.; Schrimpf, A. E.; Boyle, M. E.; Schatz, P. N. *J. Phys. Chem.* **1989**, *93*, 2999.

(11) Metcalf, D. H.; VanCott, T. C.; Snyder, S. W.; Schatz, P. N.; Williamson, B. E. *J. Phys. Chem.* **1990**, *94*, 2828.

(12) Edwards, L.; Gouterman, M. *J. Mol. Spectrosc.* **1970**, *33*, 292.

(13) Henriksson, A.; Roos, B. O.; Sundbom, M. *Theor. Chim. Acta* **1972**, *27*, 303.

(14) Stillman, M. J. In *Phthalocyanines: Properties and Applications*; Leznoff, C. C., Lever, A. B. P., Eds.; VCH Publishers: New York, 1993; Vol. III, Chapter 5; pp 227−296.

(15) Liang, X. L.; Flores, S.; Ellis, D. E.; Hoffman, B. M.; Musselman, R. L. *J. Chem. Phys.* **1991**, *95*, 403.

(16) Guo, L.; Ellis, D. E.; Hoffman, B. M.; Ishikawa, Y. *Inorg. Chem.* **1996**, *35*, 5304.

(17) Rosa, A.; Baerends, E. J. *Inorg. Chem.* **1994**, *33*, 584−595.

(18) Toyota, K.; Hasegawa, J.; Nakatsuji, H. *J. Phys. Chem. A* **1997**, *101*, 446.

(19) Rosa, A.; Ricciardi, G.; Baerends, E. J.; van Gisbergen, S. J. A. *J. Phys. Chem. A* **2001**, *105*, 3311.

(20) Casida, M. E. In *Recent Advances in Density Functional Methods*; Chong, D. P., Ed.; World Scientific: Singapore, 1995; Vol. 1; p 155.

(21) Casida, M. E. In *Recent Developments and Applications of Modern Density Functional Theory*; Seminario, J. M., Ed.; Elsevier: Amsterdam, 1996.

(22) Petersilka, M.; Gossmann, U. J.; Gross, E. K. U. *Phys. Rev. Lett.* **1996**, *76*, 1212.

(23) Petersilka, M.; Gross, E. K. U. *Int. J. Quantum Chem. Symp.* **1996**, *30*, 181.

(24) Jamorski, C.; Casida, M. E.; Salahub, D. R. *J. Chem. Phys.* **1996**, *104*, 5134.

(25) Bauernschmitt, R.; Ahlrichs, R. *Chem. Phys. Lett.* **1996**, *256*, 454.

(26) Stratmann, R. E.; Scuseria, G. E.; Frisch, M. J. *J. Chem. Phys.* **1998**, *109*, 8218.

(27) Bauernschmitt, R.; Ahlrichs, R.; Hennrich, F. H.; Kappes, M. M. *J. Am. Chem. Soc.* **1998**, *120*, 5052.

(28) van Gisbergen, S. J. A.; Groeneveld, J. A.; Rosa, A.; Snijders, J. G.; Baerends, E. J. *J. Phys. Chem. A* **1999**, *103*, 6835.

(29) Rosa, A.; Baerends, E. J.; van Gisbergen, S. J. A.; van Lenthe, E.; Groeneveld, J. A.; Snijders, J. G. *J. Am. Chem. Soc.* **1999**, *121*, 10356.

(30) van Gisbergen, S. J. A.; Rosa, A.; Ricciardi, G.; Baerends, E. J. *J. Chem. Phys.* **1999**, *111*, 2505.

(31) Ricciardi, G.; Rosa, A.; van Gisbergen, S. J. A.; Baerends, E. J. *J. Phys. Chem. A* **2000**, *104*, 635.

(32) Gross, E. K. U.; Kohn, W. *Adv. Quantum Chem.* **1990**, *21*, 255.

(33) Gross, E. K. U.; Ullrich, C. A.; Gossmann, U. J. *Density Functional Theory of Time-Dependent Systems*; Plenum: New York, 1995; Vol. 337 of NATO ASI Ser. B., p 149.

(34) Gross, E. U. K.; Dobson, J. F.; Petersilka, M. Density Functional Theory. In *Springer Series "Topics in Current Chemistry"*; Nalewajski, R. F., Ed.; Springer: Heidelberg, 1996.

(35) van Gisbergen, S. J. A.; Snijders, J. G.; Baerends, E. J. *J. Chem. Phys.* **1995**, *103*, 9347.

(36) van Gisbergen, S. J. A.; Snijders, J. G.; Baerends, E. J. *Comput. Phys. Commun.* **1999**, *118*, 119.

(37) van Gisbergen, S. J. A.; Snijders, J. G.; Baerends, E. J. *Phys. Rev. Lett.* **1997**, *78*, 3097−3100.

(38) van Gisbergen, S. J. A.; Snijders, J. G.; Baerends, E. J. *J. Chem. Phys.* **1998**, *109*, 1064.

(39) Vosko, S. H.; Wilk, L.; Nusair, M. *Can. J. Phys.* **1980**, *58*, 1200.

(40) Gritsenko, O. V.; Schipper, P. R. T.; Baerends, E. J. *Chem. Phys. Lett.* **1999**, *302*, 199.

(41) Schipper, P. R. T.; Gritsenko, O. V.; van Gisbergen, S. J. A.; Baerends, E. J. *J. Chem. Phys.* **2000**, *112*, 1344.

(42) van Leeuwen, R.; Baerends, E. J. *Phys. Rev. A* **1994**, *49*, 2421.

(43) Gritsenko, O. V.; van Leeuwen, R.; van Lenthe, E.; Baerends, E. J. *Phys. Rev. A* **1995**, *51*, 1944−1954.

(44) Baerends, E. J.; Ellis, D. E.; Ros, P. *Chem. Phys.* **1973**, *2*, 41.

(45) te Velde, G.; Baerends, E. J. *J. Comput. Phys.* **1992**, *99*, 84.

(46) Fonseca Guerra, C.; Visser, O.; Snijders, J. G.; te Velde, G.; Baerends, E. J. Parallelisation of the Amsterdam Density Functional Program. In *Methods and Techniques for Computational Chemistry*; Clementi, E.; Corongiu, G., Eds.; STEF: Cagliari, 1995; pp 305−395.

(47) ADF "STO basis set database available on line at http://tc.chem.vu.nl/SCM/Doc/atomicdatabase".

(48) Scheidt, W. R.; Dow, W. *J. Am. Chem. Soc.* **1977**, *99*, 1101.

(49) Huang, T.-H.; Rieckhoff, K. E.; Voigt, E. M. *J. Chem. Phys.* **1982**, *77*, 3424.

(50) Ough, E. A.; Nyokong, T.; Creber, K. A.; Stillman, M. J. *Inorg. Chem.* **1988**, *27*, 2724.

(51) Mack, J.; Stillman, M. J. *Inorg. Chem.* **1997**, *36*, 413.

(52) Orti, E.; Brédas, J. L. *J. Am. Chem. Soc.* **1992**, *114*, 8669.

(53) Rückmann, I.; Zeug, A.; Herter, R.; Röder, B. *Photochem. Photobiol.* **1997**, *66*, 576.

(54) Ferraudi, G. Phosphorescence of ZnPc. In *Phthalocyanines: Properties and Applications*; Leznoff, C. C.; Lever, A. B. P., Eds.; VCH: New York, 1989; Vol. I.